Influence of the Rubber Crosslinking Density of a Core–Shell Structure Modifier on the Properties of Toughened Poly(methyl methacrylate)

Y. Gui,[1,2] S. L. Sun,[2] Y. Han,[2] H. X. Zhang,[2] B. Y. Zhang[1]

[1]*Centre for Molecular Science and Engineering, Northeast University, Liaoning 110004, People's Republic of China*
[2]*School of Chemical Engineering, Changchun University of Technology, Changchun 130012, People's Republic of China*

Received 14 January 2009; accepted 23 July 2009
DOI 10.1002/app.31176
Published online 14 October 2009 in Wiley InterScience (www.interscience.wiley.com).

ABSTRACT: Four kinds of core–shell structure acrylic impact modifiers (AIMs) with different rubber crosslinking densities were synthesized. The effects of the rubber crosslinking density of the AIMs on the crack initiation and propagation resistance and the mechanical properties of the AIM/poly(methyl methacrylate) (PMMA) blends were investigated, and we found that the maximum stress intensity factor, crack propagation energy, and Izod impact strength reached maximums when the appropriate rubber crosslinking density of AIM, 2.51×10^{25} crosslinks/m^3, was adopted. Transmission electron microscopy photographs of the AIM/PMMA blends showed that the AIMs dispersed uniformly in the PMMA matrix. Meanwhile, through the analysis of optical photos and scanning electron microscopy of the impact fracture surface, we found that the deformation mechanism of the AIM/PMMA blends was local matrix shear yielding initiated by rubber particle cavitation of the AIM. The rubber of the AIM, whose crosslinking density was 2.51×10^{25} crosslinks/m^3, was beneficial to the formation of intensive voids and initiated the local shear yielding of nearby modifiers of the PMMA matrix effectively in impact tests, which led to higher Izod impact strengths. © 2009 Wiley Periodicals, Inc. J Appl Polym Sci 115: 2386–2393, 2010

Key words: core-shell polymers; shear; strength; toughness

INTRODUCTION

Poly(methyl methacrylate) (PMMA) is a typical brittle thermoplastic with excellent optical characteristics and aging behaviors. A frequently used strategy to overcome its poor impact resistance without damage to the transparency is the blending of specially designed and preformed acrylic impact modifiers (AIMs) into the matrix,[1–5] and it has been found that the optimal particle size for the toughening of PMMA is about 250 nm.[6–10] The deformation mechanism of rubber-toughened poly(methyl methacrylate) (RT-PMMA) is influenced by the strain rate, specimen geometry, and test methods. The mechanical performance of RT-PMMA is influenced by many factors, including the concentration and crosslinking density of the rubber, size and morphology of the rubber particles, interfacial adhesion between modifiers, and matrix and interparticle spacing.[5–19] Some publications[20–27] have established models for the cavitations of rubber particles of rubber-toughened polymers on the basis of energy conservation. There are a number of techniques available to investigate cavitation, including electron microscopy, X-ray scattering, light scattering, and volume measurements.[28–30] However, little attention has been paid to the effect of rubber particles' crosslinking density in AIM/PMMA blends on the mechanical properties and deformation mechanism. In this study, four kinds of designed AIMs with different rubber crosslinking densities, which were characterized by dynamic mechanical analysis and theoretical calculation, were synthesized by seed emulsion polymerization. The Izod impact strengths and bending strengths of single-edge-notched bending (SENB) specimens of the AIM/PMMA blends were measured, and optical photos and scanning electron microscopy (SEM) were used to observe the morphology of the fracture surface. The relationship between the microdeformation mechanism and the mechanical properties of RT-PMMA are discussed in detail.

EXPERIMENTAL

Materials

Methyl methacrylate (MMA), *n*-butyl acrylate (BA), ethyl acrylate (EA), and styrene (St), used as a monomer for preparation of the AIMs, were kindly supplied by Jilin Petrochemical Co. (Jilin, China).

Correspondence to: B. Y. Zhang (baoyanzhang@hotmail.com).

TABLE I
Recipes of AIMs and Diameters of Rubber Particles

	Composition of the rubber particles			Composition of the shell		Diameter of the rubber particles (nm)
	BA (g)	St (g)	EGDMA (g)	MMA (g)	EA (g)	
AIM-1	213	49	1.0	27	3	249
AIM-2	213	49	2.0	27	3	258
AIM-3	213	49	2.5	27	3	252
AIM-4	213	49	3.0	27	3	254

The monomers were distilled under nitrogen at a reduced pressure and stored at a low temperature. Ethylene glycol dimethacrylate (EGDMA; Yong Zheng Co., Shanghai, China), sodium dodecyl sulfate (SDS; Yuanju Bio-Tech Co., Shanghai, China), and potassium persulfate ($K_2S_2O_8$; Yumei Co., Shanghai, China) were used as received. The PMMA was a commercial product of Chi Mei Corporation (Taiwan, China), designated as CM211, with a number-average molecular weight of 45,218 g/mol and a weight-average molecular weight of 77,905 g/mol, as measured by gel permeation chromatography.

Preparation of the AIMs

The preparation of the core–shell structure AIMs were carried out in two stages. During the first stage, crosslinked poly(butyl acrylate-*co*-styrene) [poly(BA-*co*-St)] rubber particles were synthesized; then, MMA and EA were grafted onto it to form the outer shell. The relative quantities of distilled deionized water, crosslinking agent (EGDMA), monomer mixture (BA and St), and emulsifier (SDS) were charged into the reactor, and the polymerization was initiated by the addition of $K_2S_2O_8$ at 80°C. The rest of the monomer mixture was continuously fed into the reactor to enlarge the diameter of the rubber particles when the seed latex was slightly blue. A 45-min interval was allowed to complete the conversion of these monomer mixtures after the completion of its addition, and metered additions of appropriate quantities of MMA, EA and initiator mixture form a glassy layer of AIMS. The prepared impact modifiers were coded as AIM-1, AIM-2, AIM-3, and AIM-4, respectively, according to the content of crosslinking agent in the rubber particles. Recipes for the preparation of the AIMs and the diameter of the poly(BA-*co*-St) rubber particles, which were measured by a 90 Plus laser particle analyzer (Brookhaven Instruments Corp., New York, USA), are summarized in Table I.

Melt blending and mechanical characterization

The dried aggregates of AIMs were blended with PMMA at 220°C on a RS75H Thermo Haake mixer (Vreden, Germany). The rotating speed and temperature were set at 60 rpm and 220°C, respectively. The contents of AIM in blends were set at 10, 20, 30, and 40 wt %, and these blends were molded into Izod and SENB bars at 220°C according to ASTM D 256 and ASTM D 5045. The Izod testing was conducted on an AJU-22 impact tester (Chengde, China) at 23°C, and SENB specimens were tested with an RGT-5A electrical testing machine (Shenzen, China) at a constant speed of 10 mm/min at 23°C.

Dynamic mechanical thermal analysis

The AIMs were compression-molded into 40 × 6 × 1 mm^3 sheets at 200°C for 5 min for dynamic mechanical thermal analysis measurement. The dynamic mechanical measurements were performed over a temperature range from −50 to 10°C at a constant heating rate of 3°C/min and a frequency of 1 Hz.

Morphological properties and optical properties

Transmission electron microscopy (TEM) samples were microtomed to 60 nm in thickness from an undeformed zone of the AIM/PMMA blends at −100°C and were stained by exposure of the ultrathin sections in the vapor of RuO_4 solution before observation. TEM (model JEM-2000EX, Tokyo, Japan) operated at 160 kV was used to examine the dispersion of AIM in PMMA matrix.

The impact-fractured surface close to the notch of the impact bar with 40 wt % AIM was coated with an aurum layer and observed by SEM (model JSM-5600, Tokyo, Japan). Meanwhile, optical digital photos were used to show the difference in the stress-whitened zone of the impact fracture surface.

The transmittance of the AIM/PMMA blends with 40 wt % AIM was measured by a Hazemeter (model WGW-01, Shanghai, China) at 23°C according to ASTM D 1003.

RESULTS AND DISCUSSION

Dynamic mechanical properties of AIMs

To investigate the influence of the crosslinking agent used in rubber polymerization on the glass-

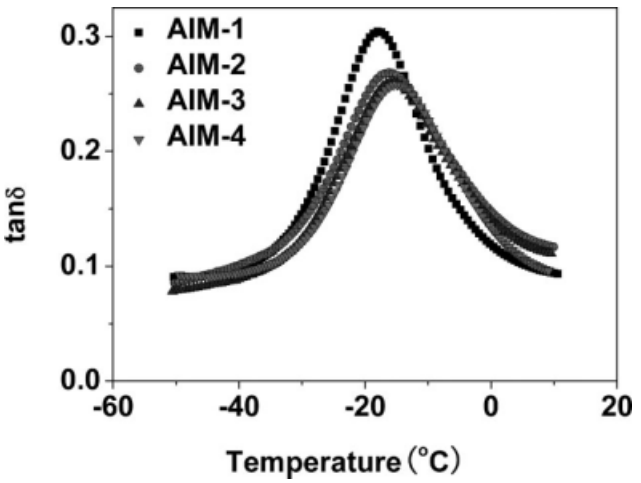

Figure 1 Tan δ as a function of temperature for AIMs with rubber phases of different crosslinking densities.

transition temperature (T_g) of the rubber phase in the AIMs, four kinds of AIMs, prepared according to the recipes shown in Table I, were studied by dynamic mechanical thermal analysis. Generally, the dynamic mechanical test of the AIMs gave two T_g values, one at a low temperature, belonging to the rubber phase of the AIMs, and another in the region of about 100°C, belonging to the poly(methyl methacrylate-*co*-ethyl acrylate) phase. In this part, only the T_g of the rubber phase was studied. As shown in Figure 1 and Table II, T_g shifted to a higher temperature step by step from AIM-1 to AIM-4. The increment of T_g was explained by the fact that the more crosslinking agent was used during the rubber particle preparation, the more crosslinkings were promoted, which constrained the mobility of the backbone segments of the molecules.

If we suppose that the crosslinking of the rubber phase of AIM was caused only by the crosslinking agent during polymerization, the crosslinking density could be calculated as follows:

$$v_x = (N_A \rho x_c)/(M_{EGDMA}) \quad (1)$$

where v_x is the crosslinking density of rubber, N_A is Avogadro's constant, ρ is the density of the rubber (1.09 g/cm^3), x_c is the weight fraction of EGDMA, and M_{EGDMA} is the molar mass of EGDMA. The values of the crosslinking density of the rubber phase and the molar content of the crosslinking agent in the rubber particles are summarized in Table III,

TABLE II
T_g Values of the Rubber Phase in Different AIMs

Type of AIM	AIM-1	AIM-2	AIM-3	AIM-4
T_g (°C)	−18.0	−16.2	−15.4	−14.9

and the results show a similar tendency to the change in T_g of the rubber phase in the AIMs.

Morphological properties and optical properties

The phase morphologies of the AIM/PMMA blends were observed by TEM, as shown in Figure 2. Poly (BA-*co*-St) rubber particles, stained by RuO_4 and shown as darkness in the photos, dispersed uniformly in the PMMA matrix, which indicated that the shell of the AIMs formed by the grafting of MMA and EA on the poly(BA-*co*-St) rubber particles had integrity and AIMs had better compatibility with the PMMA matrix. The size of the AIMs, shown in Figure 2, was consistent with the results measured by the laser particle analyzer, as shown in Table I. The results showed that all four kinds of AIM, with crosslinking densities shown in Table III, retained their morphology and size after melt blending with PMMA and subsequent molding of the blends.

The transmittance of the AIM/PMMA blends with 40 wt % AIM is shown in Table IV. The difference in the transparency of the AIM/PMMA blends was not remarkable, which indicated that the transparency of the AIM/PMMA blends had little correlation with the rubber crosslinking densities of the AIMs.

Fracture characterization

SENB tests were carried out to characterize the crack initiation and propagation behavior influenced by the rubber crosslinking density of the AIMs in this research. The schematic of the force–displacement curve obtained by the SENB tests of single-edge-notched specimens is shown in Figure 3.

Figure 3 illustrates the proportions of the crack initiation energy (U_{init}) and crack propagation energy (U_{prop}) in the total energy consumed in SENB tests. U_{prop} can be measured by the area under the force–displacement curve for the load larger than the maximum load as shown in Figure 3.

TABLE III
Molar Contents of the Crosslinking Agent and Crosslinking Density of the Rubber Phase in the AIMs

Type of AIM	AIM-1	AIM-2	AIM-3	AIM-4
Molar content of the crosslinking agent in the rubber phase (mol %)	0.24	0.47	0.59	0.70
Crosslinking density of the rubber phase (crosslinks/m^3)	1.26×10^{25}	2.51×10^{25}	3.13×10^{25}	3.75×10^{25}

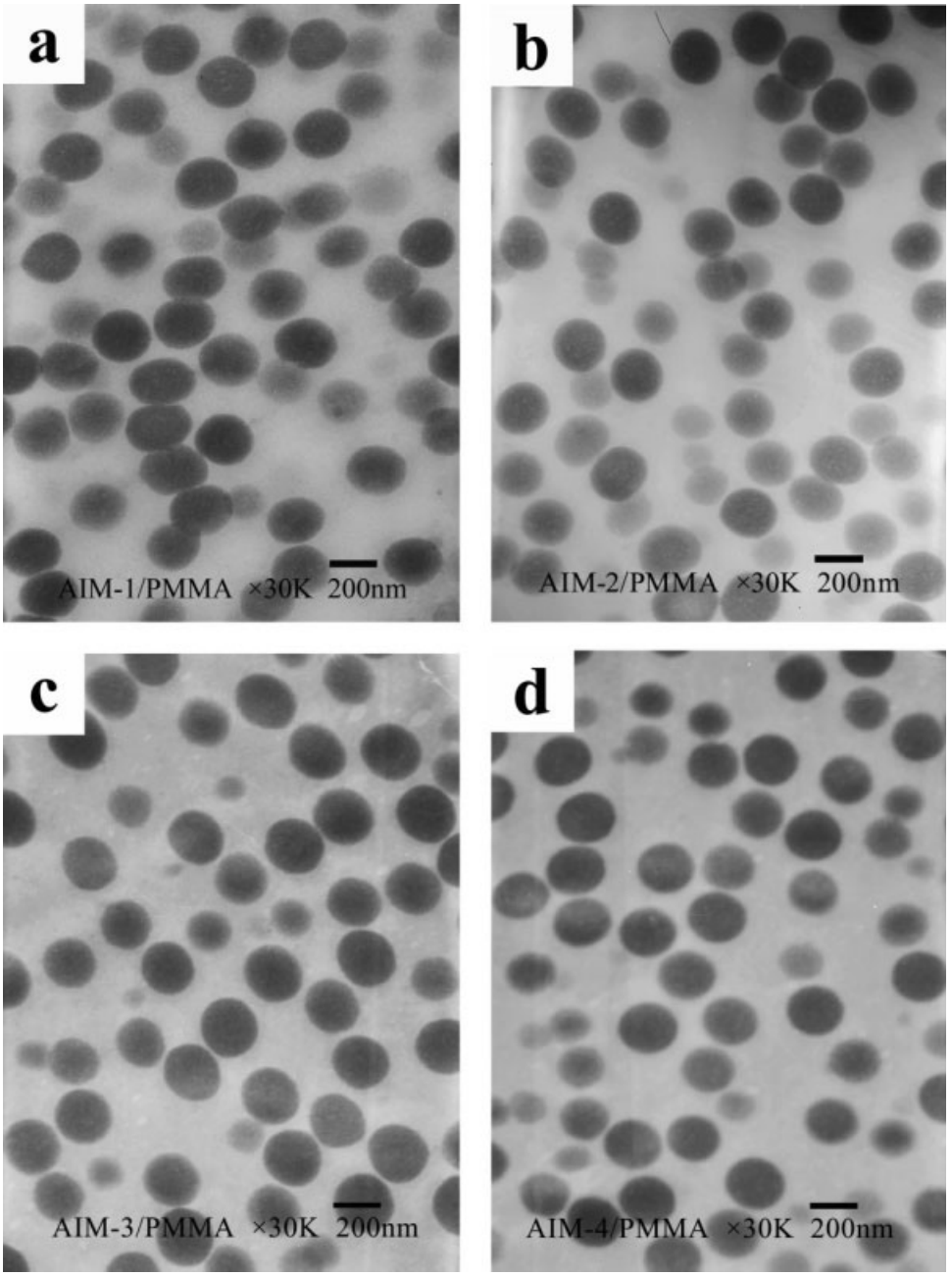

Figure 2 TEM photographs of AIM/PMMA blends containing 40 wt % AIM: (a) AIM-1/PMMA, (b) AIM-2/PMMA, (c) AIM-3/PMMA, and (d) AIM-4/PMMA.

According to ASTM 5045, mode I fracture, which pulls the preformed crack open, is one of the classic modes of fracture, and K_{IC} is the mode I critical stress intensity factor for characterizing the resistance of material to fracture, such as U_{init} shown in Figure 3. The calculation of K_{IC} should strictly meet with linear elastic fracture mechanics (LEFM) conditions. However, in this study, the fracture behavior of the AIM/PMMA blends did not meet the conditions, except for 10 wt % AIM. Therefore, $P_{\max}$ replaced the calibrated load for calculating the maximum stress intensity factor ($K_{\max}$) of the AIM/PMMA by eq. (2). Obviously, $K_{\max}$ is not an intrinsic material parameter, but it remained a useful quantity for comparing the crack initiation ability of the AIM/PMMA blends:

TABLE IV
Transmittance of the AIM/PMMA Blends with 40 wt % AIM

	AIM-1/PMMA	AIM-2/PMMA	AIM-3/PMMA	AIM-4/PMMA
Transmittance (%)	89.4	88.6	88.3	89.1

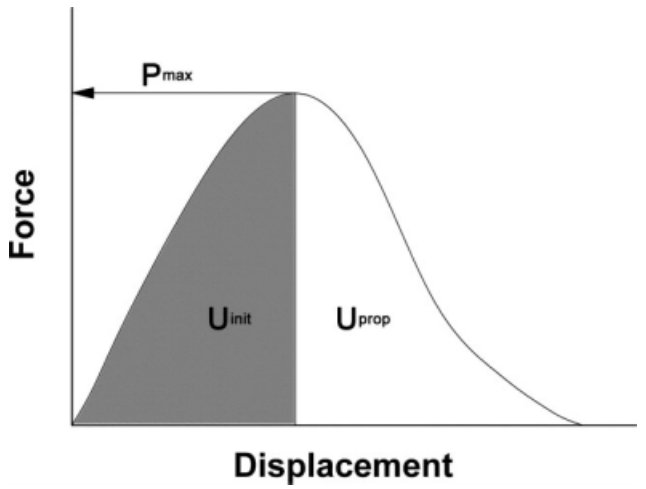

Figure 3 Schematic of the force–displacement curve of the SENB test.

$$K_{\max} = \left(\frac{P_{\max}}{BW^{1/2}}\right) f(x) \tag{2}$$

where B is the thickness of the specimen and W is its width. $f(x)$ is given by

$$f(x) = \frac{6x^{1/2}[1.99 - x(1-x)(2.15 - 3.93x + 2.7x^2)]}{(1+2x)(1-x)^{3/2}} \tag{3}$$

where x is a/W and a is the crack length.

The force–displacement curve of AIM/PMMA with 10 wt % AIM by the SENB test is shown in Figure 4. The $K_{\max}$ and U_{prop} values of the AIM/PMMA blends calculated by the previous formula are shown in Figures 5 and 6. In Figure 5, $K_{\max}$ is plotted as a function of the AIM concentration for

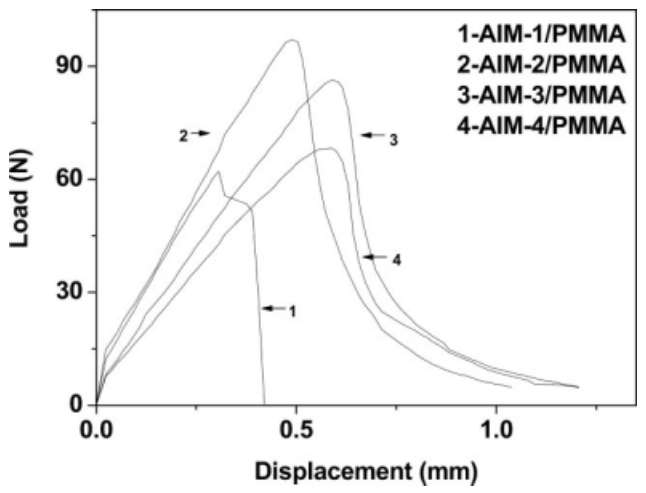

Figure 4 Force–displacement curve of AIM/PMMA with 10 wt % AIM obtained with the SENB test.

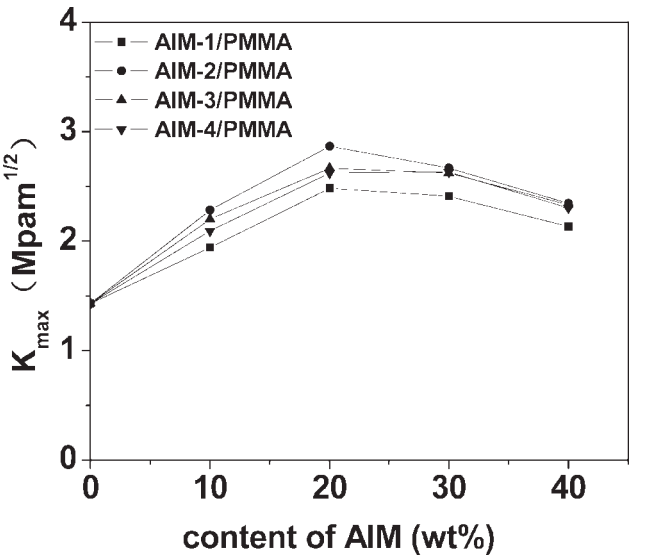

Figure 5 Effect of the AIM content on $K_{\max}$.

different AIM/PMMA blends. $K_{\max}$ of the blends increased with the AIM concentration first and reached a maximum value when the AIM content was 20%, which was about two times that of pure PMMA, and then decreased slightly as the AIM concentration increased further. At the same AIM concentration of AIM/PMMA blends, $K_{\max}$ of the AIM-2/PMMA blends was higher than the others.

Williams[31] investigated the influence of viscoelastic and thermal effects on crack growth in PMMA and attributed the strain rate dependence of K_{IC} to the viscoelastic properties and strain rate sensitive modulus of PMMA, and the critical stress intensity factor K_{IC} was given by

$$K_{IC} = u_c \sigma_y E \tag{4}$$

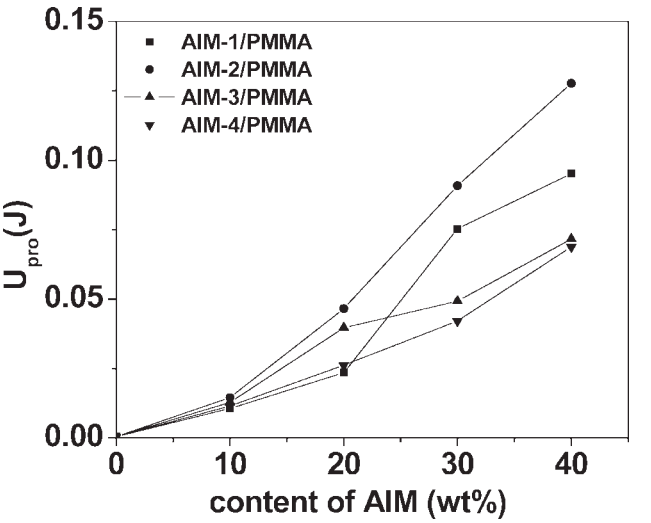

Figure 6 Effect of the AIM concentration on U_{prop}.

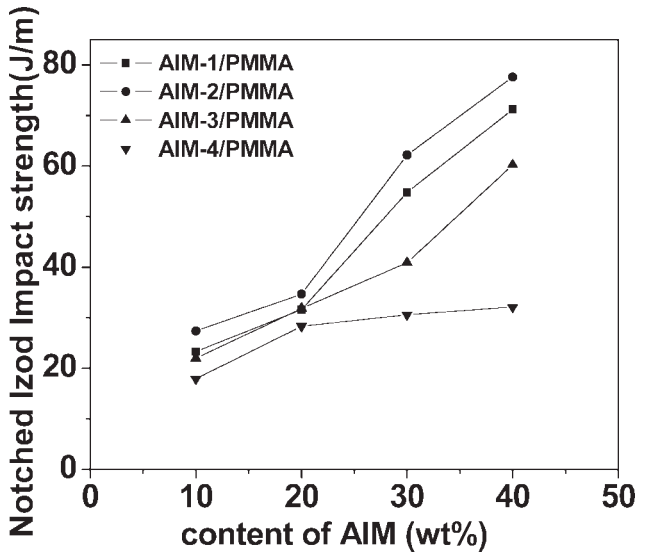

Figure 7 Izod impact strength versus the AIM content in the AIM/PMMA blends.

where u_c is the critical crack tip displacement, σ_y is the yield stress, and E is Young's modulus. Generally, E of a rubber-modified polymer blends decreases with increasing rubber concentration in SENB tests. In this research, K_{IC} was replaced by K_{max} to character the crack initiation ability, as mentioned previously. So, the variance of K_{max} with the content of AIM shown in Figure 5 may be explained by eq. (4) as followed: at lower AIM concentrations, K_{max} of the blends increased because the increase in σ_y outweighed the decrease in the product of E and u_c, and with the further increase of the AIM concentration, σ_y and E of the AIM/PMMA blends decreased notably, and that led to the decrease of K_{max}. Meanwhile, at the same AIM concentration, the difference in E of AIM, caused by the crosslinking density of the rubber phase, had little effect on E and u_c of the AIM/PMMA blends, and σ_y became a key factor for controlling K_{max} of the AIM/PMMA blends. Thus, the AIM-2/PMMA blends, with higher σ_y than the other AIM/PMMA blends, showed the highest K_{max}.

As shown in Figure 6, U_{prop} of the AIM/PMMA blends increased monotonously with increasing AIM concentration. This indicated that the resistance of crack propagation increased when more AIM particles were added to PMMA. Meanwhile, at the same AIM concentration, U_{prop} of the AIM-2/PMMA blends reached the highest values. This suggested that the rubber phase of AIM-2 with appropriate crosslinking density could have hindered crack propagation efficiently in the process of blend fracture by rubber particle cavitation and PMMA matrix yielding.

Figure 7 shows the effect of the AIM concentration on the Izod Impact strength of the different AIM/PMMA blends. The Izod impact strength of the AIM/PMMA blends increased with increasing AIM concentration, and the stress-whitening zone enlarged simultaneously, as shown in Figure 8. At the same AIM concentration, the AIM-2/PMMA blends showed a higher Izod impact strength than the others, and Figure 8 shows that the whitening zone diminished with increasing rubber crosslinking density of AIM, especially for blends with a 40 wt % AIM content.

The fracture surface, close to the notch of the Izod impact specimen with a 40 wt % AIM concentration, was observed by SEM. Voids generated by rubber cavitation dispersed on the fracture surface, and the size of the voids shown in Figure 9(a) was comparable to the rubber particle diameter of AIM-1, whereas some larger voids are shown in Figure 9(b–d). Bucknall et al.[3] did not observe any change in the volumetric strain during a creep test of RT-PMMA, and Milios et al.,[32] via investigation of the crack propagation behavior under high-speed testing, concluded that RT-PMMA deformed mainly by the shear yielding process. Kilwon et al.[17] investigated the effect of the rubber particle size on the toughening behavior of RT-PMMA under different fracture test methods. They found that the shear yielding induced by cavitation of the rubber particles was the predominant deformation mechanism in the impact tests of RT-PMMA. Thus, the larger voids could be attributed to the original voids, which were formed by the cavitation of the rubber particles of the AIM, enlarged by relaxed hydrostatic stress, which induced the shear yielding of the PMMA matrix in the vicinity of the AIMs. Figure 9(b) shows many more voids on the surface of AIM-2/PMMA than in the other blends, but their distribution was uneven. Some regions included intensive voids arranged in a line, and the others had little voids. We assumed that the onset of cavitation of some particles relieved the hydrostatic stress stored in the rubber and increased the local volume strain of particles near the critical cavitational strain so as to initiate more void formation, and the voids were arranged along the preferred direction.

Some reports[6,20–22] have proposed models on the basis of the energy balance corresponding to a cavitation criterion, which agreed with the volume strain energy stored in a particle as the driving force for

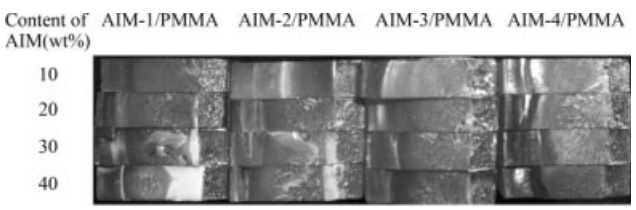

Figure 8 Typical fracture surfaces of AIM/PMMA Izod impact specimens.

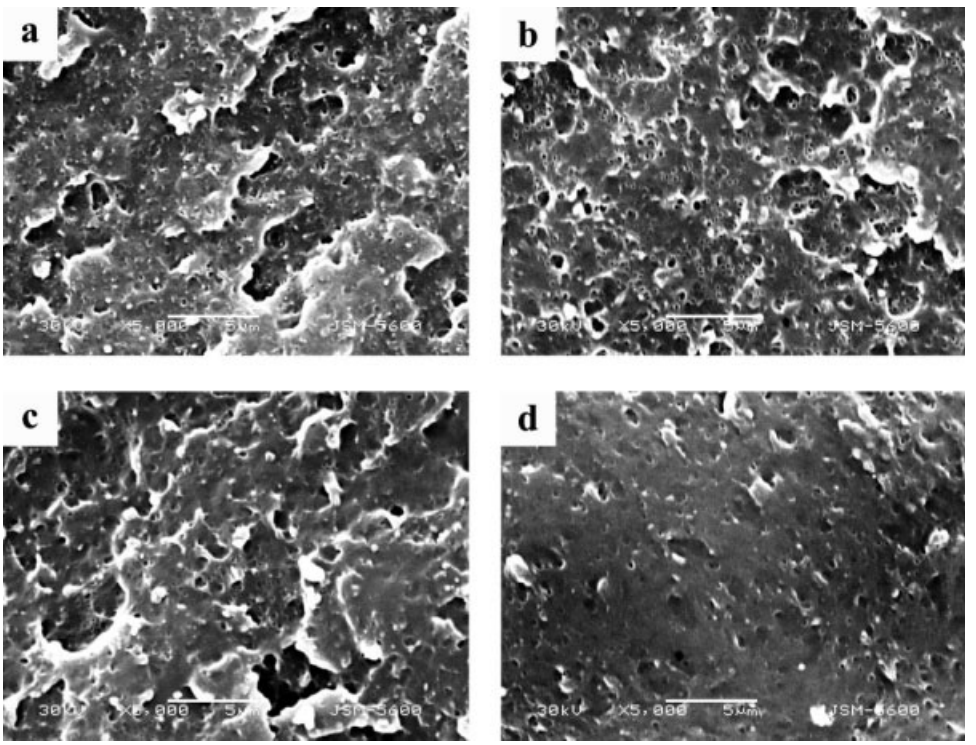

Figure 9 SEM photographs of the Izod fracture surfaces of AIM/PMMA blends containing 40 wt % AIM: (a) AIM-1/PMMA, (b) AIM-2/PMMA, (c) AIM-3/PMMA, and (d) AIM-4/PMMA.

rubber cavitation. The relationship between the volume strain energy and the properties of rubber, such as bulk modulus, shear modulus, and chain scission surface energy per unit area, was set up. Shah[33] investigated the morphological features of the fracture surfaces of notched Izod bars of RT-PMMA and attributed the features on the fracture surface to shear yielding at a higher particle concentration.

In this research, with the increase in the rubber crosslinking density from AIM-1 to AIM-4, we believe that the bulk modulus, shear modulus, and chain scission surface energy per unit area of rubber phase of the AIMs were enhanced. Meanwhile, the energy consumed in single rubber particle cavitation and relaxed hydrostatic stress increased simultaneously in the process of the Izod impact tests of the AIM/PMMA blends, which hindered easy void formation. However, impact strength was determined not only by the number of cavitations of rubber particles but also by the magnitude of relaxed hydrostatic stress, which induced more energy absorbed by the matrix deformation. So, the higher impact strength of AIM-2/PMMA, shown in Figure 7, was explained by the fact that the crosslinking density of the AIM-2 rubber phase was beneficial to the formation of intensive voids in the stress-whitening zone and relieved higher hydrostatic stress, which induced matrix shear yielding in the vicinity of the modifiers, and more total energy was consumed in the impact tests.

In the AIM-1/PMMA blends, the lower rubber crosslinking density of AIM-1 led to massive rubber cavitation and formed the biggest stress-whitening zone near the notch, as shown in Figure 7, but matrix deformation consumed less energy because of the lower relaxed hydrostatic stress of AIM-1, so it showed a low impact strength. The lower impact strength of AIM-3/PMMA and AIM-4/PMMA may have been due to the energy initiated by the rubber cavitation of AIM-3 and AIM-4, which exceeded the volume strain energy during impact tests, and only a few rubber particles formed voids on the impact fracture surface, which was proven by the smooth fracture surface shown in Figure 9(c,d).

CONCLUSIONS

The influence of the rubber crosslinking density of AIM on the properties of toughened PMMA was investigated in this study. The results demonstrate that the AIM-2/PMMA blends, in which AIM-2 had an appropriate rubber crosslinking density, presented the highest K_{max} and U_{prop} values in the SENB tests, and they showed higher notched impact strengths than the other AIM/PMMA blends. According to the results of the Izod impact tests and morphological analysis of the impact specimen fracture surfaces, we suggest that the rubber crosslinking density of AIM influenced not only the number

of cavitations of rubber particles in the blends but also the magnitude of the relaxed hydrostatic stress, which led to changes in the total energy consumed in the process of impact bar fracture.

References

1. Lovell, P. A.; McDonald, J.; Saunders, D. E.; Young, R. J. Polymer 1993, 34, 61.
2. Lovell, P. A.; Sherratt, M. N.; Young, R. J. In Toughened Plastics II: Novel Approaches in Science and Engineering; Riew, C.K.; Kinloch, A. J., Eds.; ACS Advances in Chemistry Series; American Chemical Society: Washington, DC, 1996; Chapter 15.
3. Bucknall, C. B.; Partridge, I. K.; Ward, M. V. J Mater Sci 1984, 19, 2064.
4. Rohm and Haas Co. Brit. Pat. BP 1340025 (1973).
5. Song, J. Y.; Kim, J. W.; Sun, K. D. J Appl Polym Sci 1999, 71, 1607.
6. Dompas, D.; Groeninckx, G. Polymer 1994, 35, 4743.
7. Wu, S. Polym Int 1992, 29, 229.
8. Gloaguen, J. M.; Heim, P.; Gaillard, P.; Lefebvre, J. M. Polymer 1992, 33, 4741.
9. Wrotecki, C.; Heim, P.; Gaillard, P. Polym Eng Sci 1991, 31, 213.
10. Wrotecki, C.; Heim, P.; Gaillard, P. Polym Eng Sci 1991, 31, 218.
11. Christopher, L. L.; Plummer, J. G.; Mason, J.-A. E.; Gerard, P. Polymer 2006, 47, 2389.
12. Lovell, P. A.; Ryan, A. J.; Sherratt, M. N.; Young, R. J Polym Mater Sci Eng 1994, 70, 155.
13. Wrotecki, C.; Heim, P.; Gaillard, P. Polym Eng Sci 1991, 31, 213.
14. Franck, O.; Lehmann, J. Colloid Polym 1986, 264, 473.
15. Chaobin, H.; Athene, M. D.; Michael, F. B. Macromolecules 1998, 31, 158.
16. Hyun, J. H.; Young, J. P.; Jeong, H. A.; Jung, H. K. Polym Int 1997, 44, 490.
17. Kilwon, C.; Jae, H. Y.; Chan, E. P. Polymer 1998, 39, 3073.
18. Plummer, C. J. G.; Bèguelin, P.; Kcusch, H. H. Polymer 1996, 37, 7.
19. Kilwon, C.; Jae, H. Y.; Chan, E. P. Polymer 1997, 38, 5161.
20. Lazzeri, A.; Bucknall, C. B. J Mater Sci 1993, 28, 6799.
21. Bucknall, C. B.; Karpodinis, A.; Zhang, X. C. J Mater Sci 1994, 29, 3377.
22. Fond, C. J Polym Sci Part B: Polym Phys 2001, 39, 2081.
23. Dompas, D.; Groeninckx, G.; Isogawa, M.; Hasegawa, T.; Kadokura, M. Polymer 1994, 35, 4750.
24. Dompas, D.; Groeninckx, G.; Isogawa, M.; Hasegawa, T.; Kadokura, M. Polymer 1994, 35, 4760.
25. Lazzeri, A.; Bucknall, C. B. Polymer 1995, 36, 2895.
26. Bucknall, C. K.; Ayre, D. S.; Dijkstra, D. J. Polymer 2000, 41, 5937.
27. Fond, C.; Gehant, S.; Schirrer, R. Polymer 2002, 43, 909.
28. Sue, H. Y. J Mater Sci 1992, 27, 3098.
29. Bubeck, R. A.; Buckley, D. J.; Kramer, E. J.; Brown, H. R. J Mater Sci 1991, 26, 6249.
30. Gehant, S.; Schirrer, R. J Polym Sci Part B: Polym Phys 1999, 37, 113.
31. Williams, J. G. Int J Fract Mech 1972, 8, 393.
32. Milios, J.; Papanicolau, F. C.; Young, R. J. Plast Rubber Proc Appl 1989, 11, 37.
33. Shah, N. J Mater Sci 1988, 23, 3623.